applied sciences

MDPI

Article

An Analytical Method and Experimental Validation of Stress Concentration Factors (SCFs) of Spherical Hulls with Opening Reinforcements Under External Pressure

Liyong Mao [1,2,*], Cong Ye [1,2,*], Shuai Liu [1,2], Wenyue Li [1,2], Yunsheng Shen [1,2] and Xuyin Jiang [1,2]

[1] China Ship Scientific Research Center, Wuxi 214082, China; vantasy17@126.com (S.L.); li_wyue@126.com (W.L.); dongtaisys@126.com (Y.S.); jxy670109727@126.com (X.J.)

[2] Taihu Laboratory of Deep-Sea Technological Science, Wuxi 214082, China

* Correspondence: maoliyong@cssrc.com.cn (L.M.); yec@vip.163.com (C.Y.)

Abstract

The presence of openings in spherical pressure hulls compromises the structural integrity and induces stress concentrations at the opening area. The strength assessment of shell openings remains a challenge in shell strength theory, even if using an approximated algorithm. While finite element analysis (FEA) is commonly employed, it is computationally prohibitive for iterative design. To address this gap, this study proposes a novel theoretical framework to calculate the Stress Concentration Factor (SCF) for spherical hulls with complex opening reinforcements under external pressure. A geometric transformation method based on the Equal Area Criterion (EAC) is established to convert complex reinforcement geometries into analytical forms. The accuracy is validated through comprehensive FEA and full-scale hydrostatic pressure tests on titanium-alloy manned hulls. The results demonstrate that the proposed method has high accuracy and exhibits excellent applicability, with deviations from experimental data generally within 5%. This study establishes a rapid assessment framework with high accuracy, providing a valuable engineering tool for deep-sea structural design.

Keywords: stress concentration factor; spherical hull; opening strength; external pressure test

1. Introduction

Deep-sea exploration is critical for scientific discovery and resource development [1]. Manned submersibles operating at extreme depths require robust pressure hulls to protect crew members from immense hydrostatic pressures. Spherical pressure vessels are widely adopted due to their superior load-bearing efficiency and uniform stress distribution characteristics [2–7]. Deep-sea pressure hulls are generally designed as spherical hulls with thickness-to-radius ratio within 0.02–0.08 to satisfy the safety requirements and material strength limitations [8–11]. The manufacture process primarily involves stamping thick plates into hemispheres, followed by welding the equatorial seam to form the final structure [12,13]. However, necessary openings for hatches and viewports induce localized stress concentration that can lead to structural failure under external pressure loading [14–17]. Consequently, effective reinforcement design is paramount to ensure operational safety. Titanium alloys, particularly TA31 and TC4ELI, are the preferred materials for deep-sea applications due to their excellent strength-to-weight ratio and corrosion resistance. Current design practices for spherical hulls with openings primarily rely on finite element analysis

Check for updates

Academic Editor: José A. Orosa García

Received: 7 May 2026
Revised: 22 June 2026
Accepted: 23 June 2026
Published: 2 July 2026

(FEA). Although FEA provides detailed stress distributions, it is computationally expensive for iterative design processes. Figures 1 and 2 illustrate the typical manned hull structure and the specific reinforcement details studied in this research.

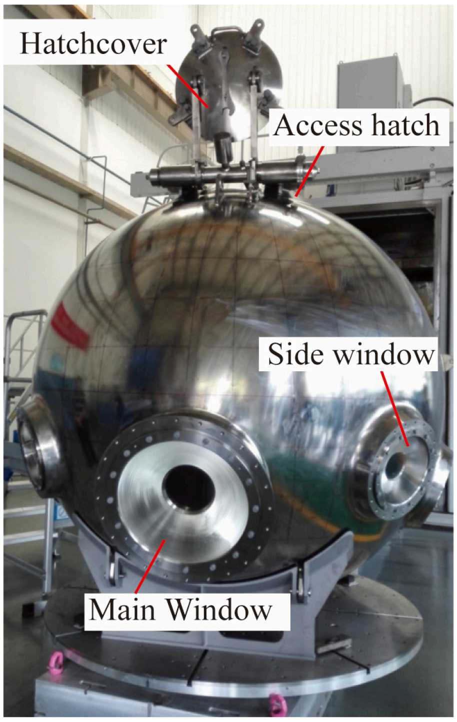

Figure 1. Manned hull with several openings.

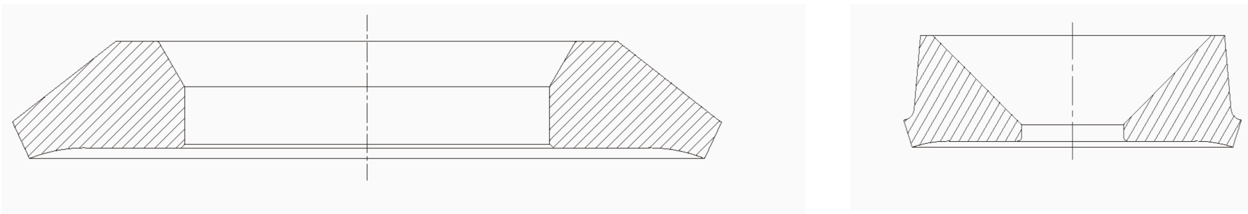

(**a**) (**b**)

Figure 2. Structure reinforcement. (**a**) Hatch. (**b**) Main window.

Previous studies have mainly focused on the structural buckling stability considering the influence of geometric imperfection [18–22]. The interaction between residual stresses and working stresses significantly diminishes the creep–fatigue life of conical-column pressure shells [23]. Fatigue assessment methods have been developed using equivalent structural stress and fatigue crack propagation approaches [24,25].

As the shell thickness and the operation depth increase, the main failure mode of the shell is both buckling failure and strength yield failure. Millet et al. [26] reviewed the reinforcement rules in different codes, while D Calligeros [27] suggested that the design rules are conservative for reinforcement of pressure vessel openings under external pressure. Xu et al. [28] derived a theoretical formula for calculating the strength of a cylindrical shell reinforcement, and this formula provides an appropriate theoretical reference for designing spherical shells with openings. Pranesh et al. [29] analyzed reinforced viewports in the pressure hull using the finite element method and suggested that the calculated primary and secondary stresses should below the permissible limits. Ma et al. [30] investigated the numerical buckling load of an externally pressurized spherical shell with a reinforced opening and verified the results using full-scale external pressure tests.

However, limited theoretical research exists on the stress concentration of spherical shells with opening reinforcement under external pressure. Existing standards, such as CCS [31], often rely on FEA for reinforcement verification, and analytical methods [28] primarily focus on cylindrical shells or internal pressure conditions. Although FEA is widely used, it is time-consuming for iterative design. To address this gap, this study proposes an analytical method to assess the opening reinforcement strength of spherical hulls, which aims to provide a generalized solution. Numerical analysis, finite element analysis and full-scale hydrostatic pressure tests on manned hulls were performed to validate the reliability and applicability of the proposed method.

2. Calculation on Theoretical Stress Concentration Factor

2.1. Geometric Transformation Based on Equal Area Criterion

For the complex reinforcement shown in Figure 2a, this paper introduces a geometric transformation of reinforcement based on the Equal Area Criterion (EAC), converting complex reinforcement geometries into analytically tractable forms. The reinforcement area of the access hatch is geometrically transformed into a wall (height unchanged) with a thick plate reinforcement (width unchanged), as shown in Figure 3a, and the reinforcement of the window openings is transformed into wall reinforcement with height unchanged. During the transformation, the main parameters, such as opening radius, plate width, wall height, and total reinforcement area, are kept unchanged. This ensures that the membrane stress characteristics of the original structure are accurately represented in the transformed model.

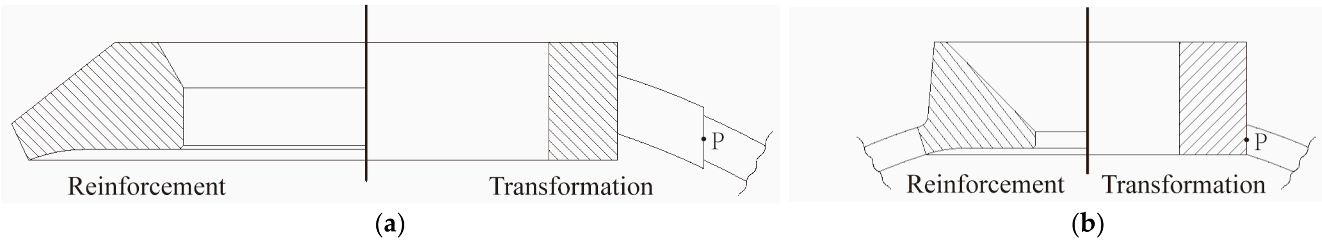

Figure 3. Transformation form. (**a**) Hatch. (**b**) Main window.

2.2. Theoretical Method

2.2.1. Wall Reinforcement

The spherical hull structure with wall reinforcement is shown in Figure 4.

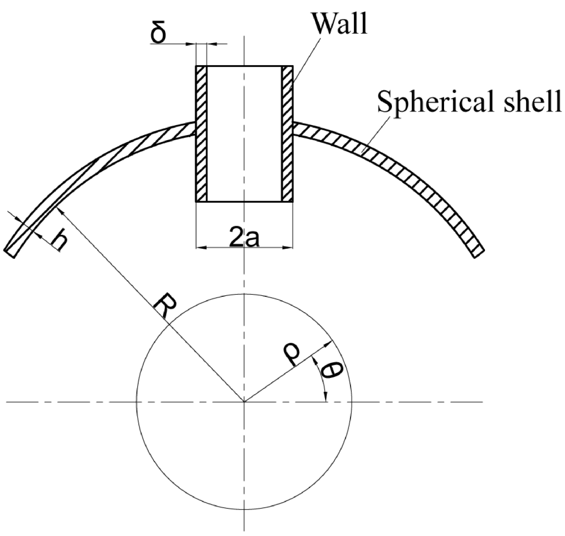

Figure 4. Spherical hull with wall reinforcement.

For a relatively small circular opening, the local reinforced region can be treated as an axisymmetric structure [32]. In the polar coordinate system (ρ, θ), the displacement and stress function of the spherical shell are written as Equation (1). The analysis assumes linear elastic material behavior, uniform external pressure, a circular or approximately circular opening, and a local stress concentration field that decays away from the opening edge [32]:

$$\begin{cases} D\Delta\Delta w + \frac{1}{R}\Delta(\Phi) - p = 0 \\ \Delta\Delta(\Phi) - \frac{Eh}{R}\Delta w = 0 \end{cases} \tag{1}$$

where D is the bending rigidity, $D = Eh^3/12\left(1-\mu^2\right)$; E is Young's modulus; μ is Poisson's ratio; R is the radius of the spherical hull; h is the spherical hull thickness; p is external pressure; w is the normal displacement function; Φ is the stress function; and Δ is the differential operator, $\Delta = \frac{\partial^2}{\partial\rho^2} + \frac{1}{\rho}\frac{\partial}{\partial\rho} + \frac{1}{\rho^2}\frac{\partial^2}{\partial\theta^2}$.

The functions of internal membrane force T, internal moments M and internal normal force N can be expressed by Φ and w, as shown in Equation (2) in the polar coordinate system frame:

$$\begin{aligned} T_\rho &= \frac{1}{\rho^2}\frac{\partial^2\Phi}{\partial\theta^2} + \frac{1}{\rho}\frac{\partial\Phi}{\partial\theta} \\ T_\theta &= \frac{\partial^2\Phi}{\partial\rho^2} \\ T_{\rho\theta} &= -\frac{1}{\rho}\frac{\partial^2\Phi}{\partial\rho\partial\theta} + \frac{1}{\rho^2}\frac{\partial\Phi}{\partial\theta} \\ M_\rho &= -D\left[\frac{\partial^2 w}{\partial\rho^2} + \mu\left(\frac{1}{\rho}\frac{\partial w}{\partial\rho} + \frac{1}{\rho^2}\frac{\partial^2 w}{\partial\theta^2}\right)\right] \\ M_\theta &= -D\left(\frac{1}{\rho}\frac{\partial w}{\partial\rho} + \frac{1}{\rho^2}\frac{\partial^2 w}{\partial\theta^2} + \mu\frac{\partial^2 w}{\partial\rho^2}\right) \\ M_{\rho\theta} &= -D(1-\mu)\left(\frac{1}{\rho}\frac{\partial^2 w}{\partial\rho\partial\theta} - \frac{1}{\rho^2}\frac{\partial w}{\partial\theta}\right) \\ N_\rho &= -D\frac{\partial}{\partial\rho}(\Delta w) \\ N_\theta &= -\frac{D}{\rho}\frac{\partial}{\partial\rho}(\Delta w) \end{aligned} \tag{2}$$

The normal displacement function w and stress function Φ should satisfy Equation (1). The stress concentration at the opening area is local features and it can be assumed that w and θ are independent owing to features of the axisymmetric structure. Since the peak stress decays rapidly with increasing distance from the opening area [32], the displacement function of a spherical hull with an opening is assumed as an exponential decay function in Equation (3):

$$w = w_0\beta^{-2} \tag{3}$$

where $\beta = \rho/a$; a is the opening radius; and w_0 is an undetermined coefficient.

Then, Φ can be solved by substituting Equation (3) into Equation (1):

$$\Phi = A\ln\rho + B\rho^2 + \frac{w_0 E h a^2}{2R}(\ln\beta)^2 \tag{4}$$

where A and B are undetermined coefficients defined by boundary conditions.

Both displacement function w and stress function Φ are functions of the undetermined coefficient w_0. And w_0 can be obtained using Equation (5) based on the energy method.

$$\iint\limits_\sigma [D\Delta\Delta w + \Delta(\Phi)/R - p]\delta w d\sigma + \int\limits_c (M_\rho - M_a)\delta\frac{dw}{d\rho}dc - \int\limits_s \left(N_\rho + \frac{pa}{2} - \frac{aT_a}{R}\right)\delta w ds = 0 \tag{5}$$

As shown in Equation (6), T_ρ and T_θ can be obtained by solving Equations (2) and (4):

$$\begin{aligned} T_\rho &= \frac{A}{\rho^2} + 2B + \frac{Ehw_0}{R}\frac{a^2}{\rho^2}\ln\frac{\rho}{a} \\ T_\theta &= -\frac{A}{\rho^2} + 2B + \frac{Ehw_0}{R}\frac{a^2}{\rho^2}\left(1-\ln\frac{\rho}{a}\right) \end{aligned} \tag{6}$$

The boundary conditions of spherical shells with openings should meet Equation (7), which enforces compatibility between the shell deformation and the reinforced boundary:

$$\begin{array}{c} T_\rho = T_a, when: \rho = a \\ T_\rho = T_\theta = \frac{pR}{2}, when: \rho \to \infty \end{array} \tag{7}$$

Then, undetermined coefficients A and B can be obtained in Equation (8), which is solved from Equations (6) and (7):

$$\begin{array}{c} A = (T_a - 2B)a^2 \\ B = \frac{pR}{4} \end{array} \tag{8}$$

where $T_a = \frac{A_c\left(1+\frac{Ehw_0}{pR^2}-\frac{a}{R}\frac{h}{\delta}\right)}{1+(1+\mu)\frac{A_c}{ah}}$ [28]; A_c is the effective area, $A_c = \zeta\delta\sqrt{a\delta}$; ζ is the effective coefficient of wall heigh [31]; and δ is wall thickness.

SCF K_ρ and K_θ can be obtained from T_ρ and T_θ using A and B, as shown in Equation (9).

$$\begin{array}{c} K_\rho = \frac{T_\rho}{pR/2} = 1 + \left[\frac{2\frac{A_c}{ah}\left(1+\overline{w}_0-\frac{ah}{R\delta}\right)}{1+\frac{A_c}{ah}(1+\mu)} - 1\right]\beta^{-2} + 2\overline{w}_0\beta^{-2}\ln\beta \\ K_\theta = \frac{T_\theta}{pR/2} = 1 + \left[1 - \frac{2\frac{A_c}{ah}\left(1+\overline{w}_0-\frac{ah}{R\delta}\right)}{1+\frac{A_c}{ah}(1+\mu)}\right]\beta^{-2} + 2\overline{w}_0\beta^{-2}(1-\ln\beta) \end{array} \tag{9}$$

where $\overline{w}_0 = Ehw_0/pR^2$.

The circumferential stress is usually the maximum at the opening edge ($\beta = 1$). The max SCF can be calculated by Equation (10):

$$(K_\theta)_{\max} = 2 - \frac{2\frac{A_c}{ah}\left(1+\overline{w}_0-\frac{ah}{R\delta}\right)}{1+\frac{A_c}{ah}(1+\mu)} + 2\overline{w}_0 \tag{10}$$

The SCF $(K_\theta)_{\max}$ of the spherical hull with wall reinforcement can be solved with simplified parameters [32], as shown in Equation (11). And the family curves are illustrated in Figure 5.

$$\begin{array}{c} (K_\theta)_{\max} = 2 - \frac{2K_1\left[1+\overline{w}_0-0.088(K_1)^{-2/3}(K_2)^{2/3}\right]}{1+1.3K_1} + 2\overline{w}_0 \\ \overline{w}_0 = \frac{1-\frac{2K_1\left[1-0.088(K_1)^{-2/3}(K_2)^{2/3}\right]}{1+1.3K_1}}{0.0078K_2^{-4}+1+\frac{2K_1}{1+1.3K_1}+2.43K_1^{5/3}K_2^{-8/3}} \end{array} \tag{11}$$

where $K_1 = \frac{A_c}{ah}$ and $K_2 = \frac{a}{R}\sqrt[4]{\frac{R}{h}}\zeta$. The substitutions K_1 and K_2 are dimensionless structural parameters introduced to make the equations more visual and easier to implement in calculation programs.

When the structural design parameters are determined, K_1 and K_2 can be calculated from the above equation, and SCF at the spherical shell opening area can be obtained from Figure 5. This enables rapid optimization of the reinforcement geometry before detailed finite element verification.

2.2.2. Wall and Thick Plate Combination Reinforcement

A thick plate should be introduced into the reinforcement structure when the wall reinforcement fails to satisfy the strength limitations, even when the wall to spherical shell ratio reaches 2.0 [30]. The spherical hull structure with the wall and thick plate combination reinforcement is illustrated in Figure 6.

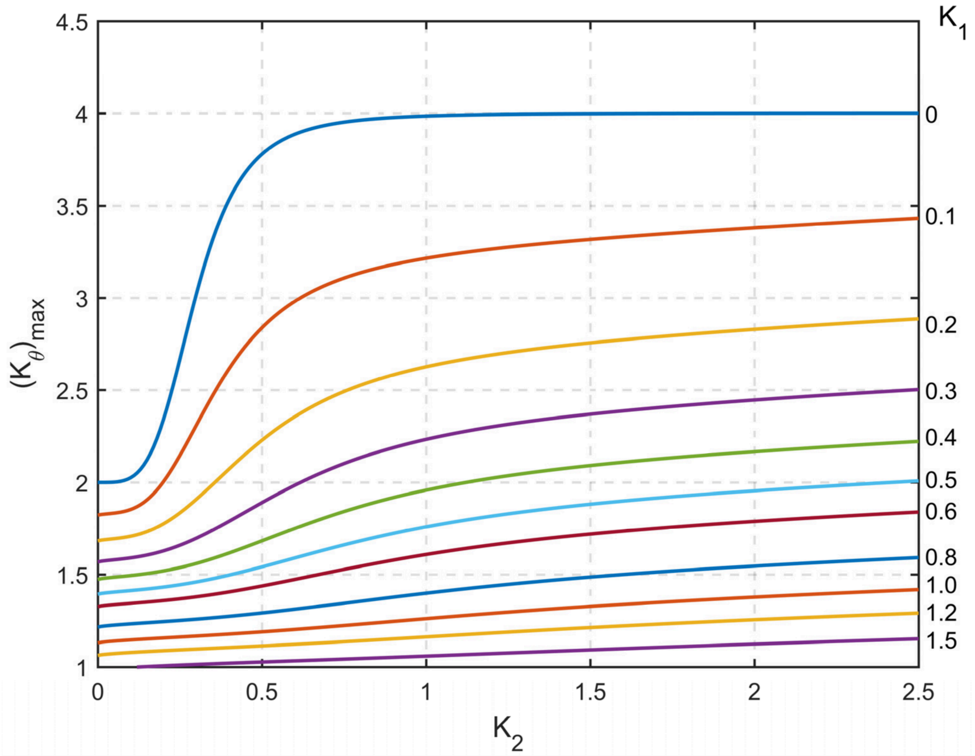

Figure 5. SCF of a spherical hull with wall reinforcement.

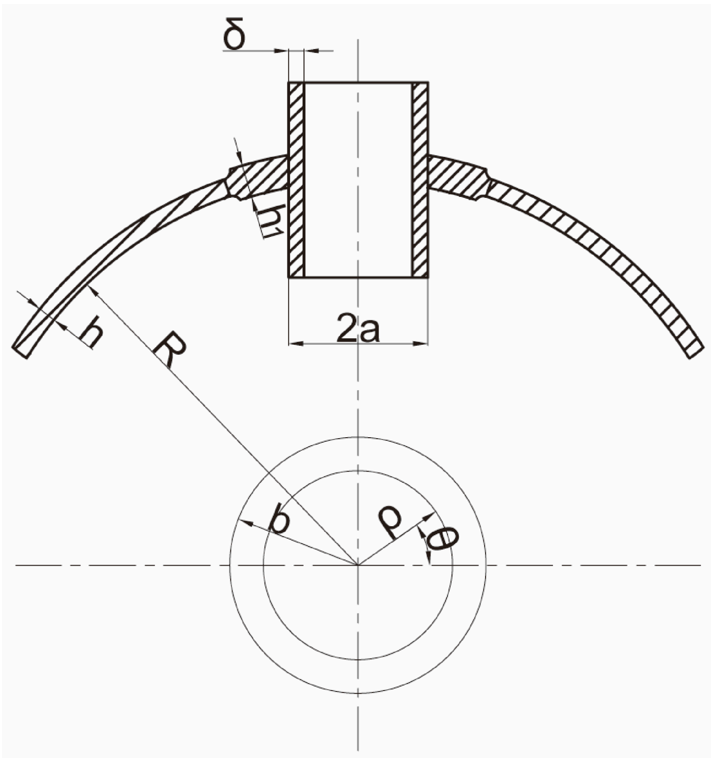

Figure 6. Spherical hull with wall and thick plate combination reinforcement.

The wall and thick plate combination reinforcement leads to stress concentration at the opening edge ($\rho = a$) and the connection between the thick plate and spherical shell ($\rho = b$) [28]. The analysis procedure incorporates the compatibility equation at the connection of the reinforcement plate and spherical shell, in addition to the boundary conditions considered in the wall reinforcement. The circumferential stress remains the primary concern, similar to the stress characteristics in the wall reinforcement [11]. The SCFs at opening edges are given in Equations (12) and (14):

- SCF at the opening for the thick plate ($\rho = a$);

$$(K_{r\theta})_{\max} = \frac{T_\theta/h_1}{pR/2h} = \frac{2}{\xi}\left[\frac{\left(m^2+1\right)\frac{T_a}{pR} - 2m^2\frac{T_b}{pR} + 2\overline{w}_0\xi\ln m}{1-m^2}\xi\overline{w}_0\right] \tag{12}$$

where $\xi = h_1/h$, $m = b/a$, b is the radius of shell opening for reinforcement plates, and h_1 is reinforcement plate thickness.

The reinforcement plate coefficient γ was introduced to link $(K_{r\theta})_{\max}$ to the SCF $(K_\theta)_{\max}$ of the wall reinforcement case, as shown in Equation (13) [32].

$$(K_{r\theta})_{\max} = \gamma(K_\theta)_{\max} = \frac{1}{1+\alpha(m-1)}(K_\theta)_{\max} \tag{13}$$

where α can be obtained from previous research [32].

- SCF at the connection of the thick plate and spherical shell:

$$(K_{s\theta})_{\max} = \frac{T_\theta}{pR/2} \tag{14}$$

Referring to Equation (4), the stress function Φ_2 of the spherical hull with combined reinforcement can be written as Equation (15).

$$\Phi_2 = A_2\ln\rho + B_2\rho^2 + \frac{w_0Eha^2}{2R}\left(\ln\frac{\rho}{a}\right)^2 \tag{15}$$

The boundary conditions of spherical shells with combined reinforcement should satisfy Equation (16):

$$\begin{aligned} T_\rho = T_b, when: \rho = b \\ T_\rho = T_\theta = \tfrac{pR}{2}, when: \rho \to \infty \end{aligned} \tag{16}$$

And undetermined coefficients A_2 and B_2 can be obtained, as shown in Equation (17):

$$\begin{aligned} A_2 &= b^2\left(T_b - \tfrac{pR}{2} - \tfrac{Ehw_0}{R}\tfrac{1}{m^2}\ln m\right) \\ B_2 &= \tfrac{pR}{4} \end{aligned} \tag{17}$$

Substituting Equation (17) into Equation (14) gives the rewritten SCF expression in Equation (18).

$$\begin{aligned} (K_{s\theta})_{\max} &= \frac{T_\theta}{pR/2} \\ &= 2 - \frac{2T_b}{pR} + \frac{2\overline{w}_0}{m^2} \end{aligned} \tag{18}$$

Internal force T_a, T_b and explicit displacement w are determined using the following three boundary conditions:

1. w fits the mixed variational equation solved from Equation (5):

$$\begin{aligned} &\left(2 - \tfrac{4\ln m}{m^2-1}\right)\tfrac{T_a}{pR} + \tfrac{4m^2\ln m}{m^2-1}\tfrac{T_b}{pR} + \left\{\left[\tfrac{40/3-8\mu}{12(1-\mu^2)}\xi^3 + \tfrac{16\left(1-\xi^3\right)}{9(1-\mu^2)}m^{-6}\right](R/a)^4(h/R)^2\right. \\ &\left.+\xi(1-m^{-2}) + m^{-2} - \tfrac{4\xi(\ln m)^2}{m^2-1} + \tfrac{8\sqrt[4]{3(1-\mu^2)}}{3(1-\mu^2)}\tfrac{1}{\xi}\left(\tfrac{R}{a}\right)^3\tfrac{A_c}{ah}\tfrac{\delta}{h}\tfrac{h}{R}\right\}\overline{w}_0 = 1 + 2\ln m \end{aligned} \tag{19}$$

where $\overline{w}_0 = Ehw_0/pR^2$.

2. The compatibility equation for connection of the wall and thick plate:

$$\left[1+\frac{(m^2+1)+\mu(m^2-1)}{m^2-1}\frac{A_c}{ah_1}\right]\frac{T_a}{pR}-\frac{2m^2}{m^2-1}\frac{A_c}{ah_1}\frac{T_b}{pR}-\left(1-\frac{2\ln m}{m^2-1}\right)\frac{A_c}{ah_1}\frac{w_0 E h_1}{pR^2}+\frac{A_c}{ah_1}\frac{a}{R}\frac{h_1}{\delta}=0 \tag{20}$$

3. The compatibility equation for the connection of the thick plate and spherical shell:

$$\frac{2}{m^2-1}T_a-\frac{(1+\mu)+m^2(1-\mu)+(m^2-1)(1+\mu)\xi}{m^2-1}T_b+\frac{\frac{2w_0 E h_1}{R}\ln m}{m^2-1}=-\xi pR \tag{21}$$

Solving Equations (19)–(21) gives T_b and w_0, as shown in Equation (22).

$$\begin{aligned} T_b &= pR\tfrac{E}{C} \\ w_0 &= \tfrac{PR^2}{Eh}\tfrac{F}{C} \end{aligned} \tag{22}$$

where

$$\begin{aligned}
E= {} & t_1 t_2\left[K_1\left(1.3m^2+0.7\right)+\xi\left(m^2-1\right)\right]+2t_1^2\ln m(2\ln m+1)\left[K_1\left(1.3m^2+0.7\right)+\xi\left(m^2-1\right)\right] \\
& +2K_1\xi(2t_1\ln m-1)^2-2t_1K_1(2\ln m+1)(2t_1\ln m-1)-0.17606t_1t_2K_1^{1/3}K_2^{2/3} \\
& -0.35212t_1K_1^{1/3}K_2^{2/3}\xi\ln m(2t_1\ln m-1) \\
F= {} & (2\ln m+1)\frac{t_1}{\xi}\left[K_1\left(1.3m^2+0.7\right)+\xi\left(m^2-1\right)\right](1.3\xi+2t_1+0.7)+4t_1K_1m^2(2t_1\ln m-1) \\
& +0.70424t_1^2K_1^{1/3}K_2^{2/3}m^2\ln m-0.17606K_1^{1/3}K_2^{2/3}(2t_1\ln m-1)(1.3\xi+2t_1+0.7) \\
& -4t_1^2K_1(2\ln m+1)\frac{m^2}{\xi}-4t_1^2m^2\ln m\left[K_1\left(1.3m^2+0.7\right)+\xi\left(m^2-1\right)\right] \\
C= {} & 8t_1^3m^2(\ln m)^2\left[K_1\left(1.3m^2+0.7\right)+\xi\left(m^2-1\right)\right]+2K_1(2t_1\ln m-1)^2(1.3\xi+2t_1+0.7) \\
& +\frac{t_1t_2}{\xi}\left[K_1\left(1.3m^2+0.7\right)+\xi\left(m^2-1\right)\right]-4\frac{t_1^2t_2}{\xi}K_1m^2-16t_1^2K_1m^2\ln m(2t_1\ln m-1) \\
t_1= {} & \frac{1}{m^2-1} \\
t_2= {} & 2.43\frac{K_1^{5/3}}{K_2^{8/3}}+\frac{0.0078\xi^3+0.015(1-\xi^3)m^{-6}}{K_2^4}+\xi\left(1-\frac{1}{m^2}\right)+\frac{1}{m^2}-4t_1\xi(\ln m)^2
\end{aligned}$$

The SCF $(K_{s\theta})_{\max}$ at the connection of the thick plate and spherical shell can be simulated in Equation (23) with known structural parameters.

$$(K_{s\theta})_{\max}=2\left(1-\frac{E-F}{C}\right) \tag{23}$$

where E, F and C are defined in Equation (22) above. Figure 7 shows part of the SCF family curves. SCF can be obtained in family curves based on K_1 and K_2 for known m and ξ. And Equation (23) degenerates to Equation (11) when $m \to 1$ and $\xi = 1$, which is the wall reinforcement case.

From Figure 7, it can be seen that as m and ξ increase, the SCF decreases. The effect of thick plate thickness h_1 and thick plate opening radius b on SCF is further analyzed in Figure 8. It can be observed that $(K_{s\theta})_{\max}$ decreases steadily, but with a gradually decreasing reduction rate, as h_1 or b increases. This trend shows a diminishing return on stress reduction by solely increasing the reinforcement dimensions. This suggests an optimal design point where the structural weight is balanced against the structural strength limitations.

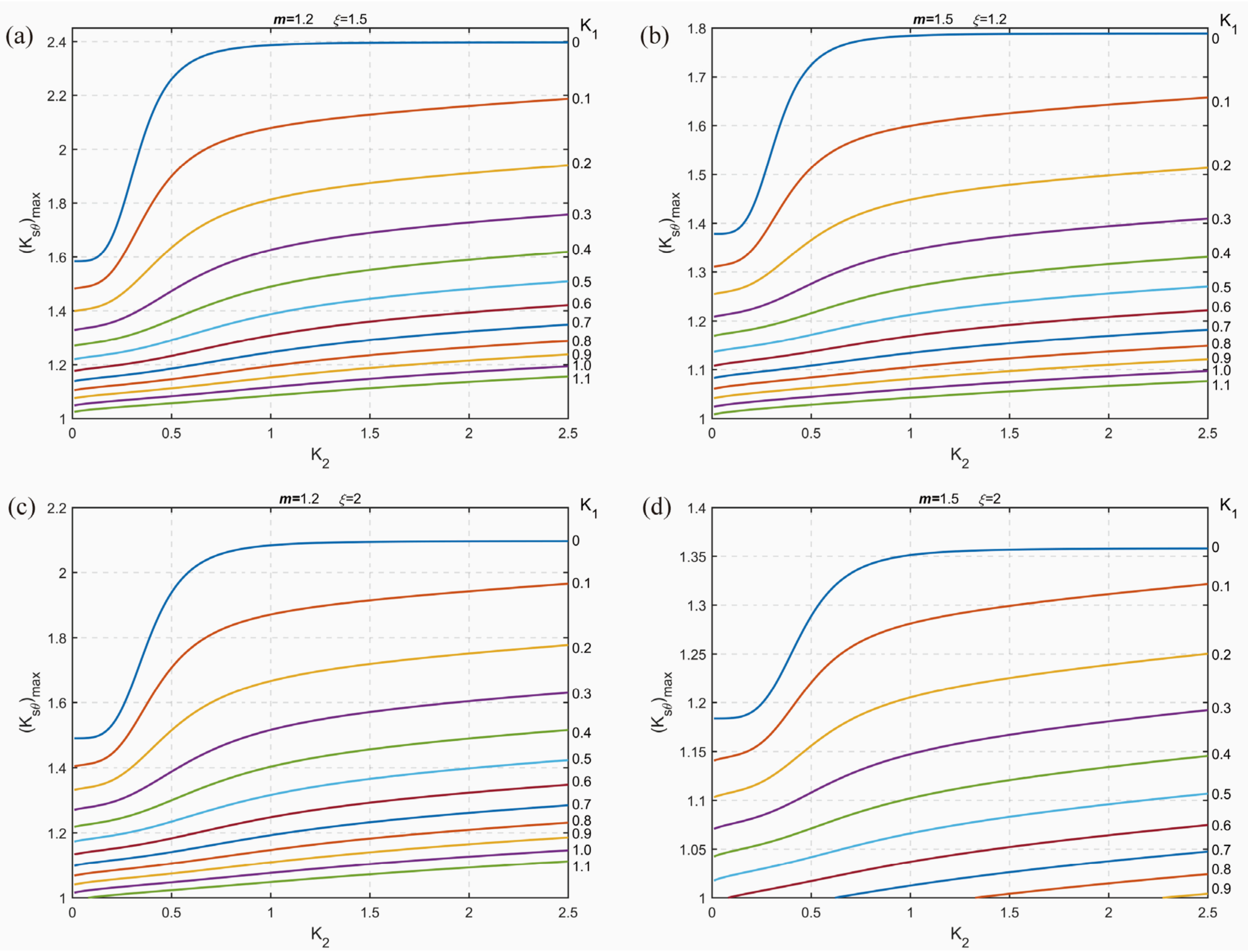

Figure 7. SCF at the connection of the thick plate and spherical shell with different structure design parameters: (**a**) $m = 1.2, \xi = 1.5$, (**b**) $m = 1.5, \xi = 1.2$, (**c**) $m = 1.2, \xi = 2$, (**d**) $m = 1.5, \xi = 2$.

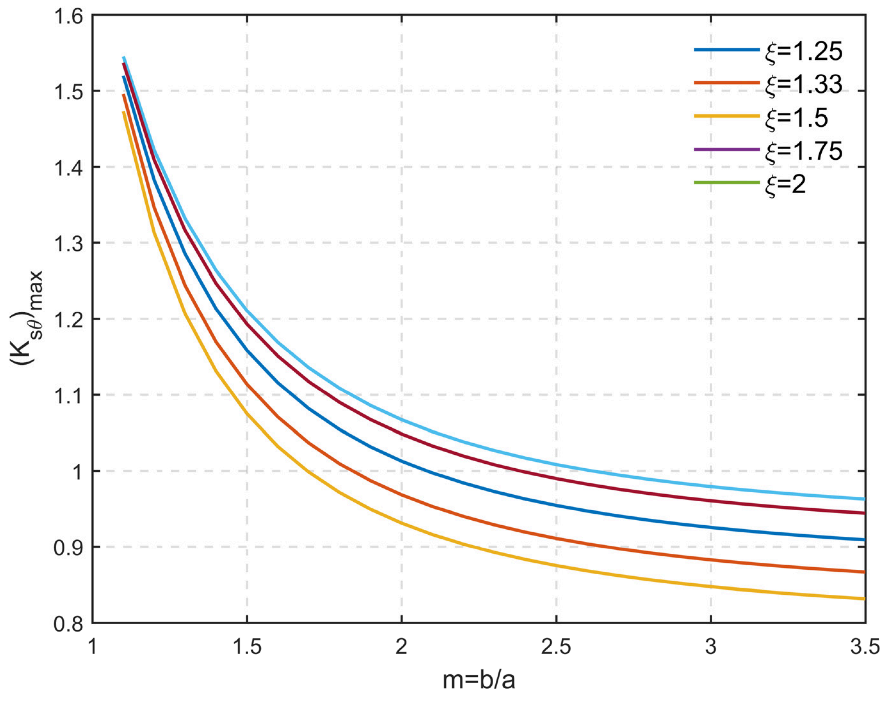

Figure 8. The effect of reinforcement plate radius and thickness on SCF.

Tables 1 and 2 show the effect of wall thickness and reinforcement plate thickness on the SCF. The SCF variation remains less than 5% when δ and h_1 vary by less than ±20%, respectively, when all the other opening reinforcement structural parameters are kept unchanged. This indicates that the transformed parameters have a limited influence on the stress concentration at the opening region. Therefore, the proposed method is well suited for strength verification of the spherical shell opening reinforcement shown in this research.

Table 1. SCF with wall thickness changing.

Material	δ	$\delta \times 1.2$	Deviation	$\delta \times 0.8$	Deviation
TA31	1.169	1.131	−3.251%	1.220	4.363%
TC4ELI	1.143	1.105	−3.325%	1.192	4.287%

Table 2. SCF with reinforcement plate thickness changing.

Material	h_1	$h_1 \times 1.2$	Deviation	$h_1 \times 0.8$	Deviation
TA31	1.169	1.121	−4.106%	1.227	4.962%
TC4ELI	1.143	1.097	−4.025%	1.198	4.812%

The stress concentration near the opening is primarily attributed to the discontinuity of membrane stress transmission and stiffness mismatch between the spherical shell and the opening reinforcements. Increasing the reinforcement plate radius or thickness can enhance the local load-transfer path and reduce the stress concentration at the opening area. However, the reduction in SCF exhibits a diminishing return as the reinforcement dimensions increase., which indicates that simply increasing reinforcement dimensions may not always be efficient. Excessive reinforcement may lead to structural weight increasing without producing proportional stress reduction. Therefore, the reinforcement design should balance opening reinforcements strength, smooth stiffness transition and structural weight. The proposed SCF method serve as a rapid preliminary design and strength-evaluating tool before detailed finite element verification. However, for non-axisymmetric openings, complex local attachments, very thick shells, or highly nonlinear deformation cases, further validation or direct finite element analysis is still required.

3. Experimental Details and Finite Element Analysis

3.1. External Pressure Test

An external pressure test was applied on two full-scale manned spherical hulls to validate the theoretical method. The primary geometric parameters are listed in Table 3. The maximum operating depth of the spherical hull is 4500 m underwater, corresponding to an operating pressure of 46 MPa. The maximum test pressure was set to 57.5 MPa (1.25 times the operating pressure).

Table 3. Structure design parameters.

Material	Inside Diameter (mm)	Thickness (mm)	Opening Radius (mm)		
			Access Hatch	Main Window	Side Window
TA31 TC4ELI	2100	56 53	330	315.7	262.9

High-sensitivity resistance strain gauges with a temperature compensation function were arranged on both sides of the spherical hulls to capture stress accurately, as shown in Figure 9. The gauges were waterproofed to ensure reliability under high-pressure conditions. Figure 10 shows the test preparation. A step-wise hydrostatic pressure test procedure was conducted up to 57.5 MPa (1.25 times the operational pressure). The loading and unloading rates were controlled at 0.6 MPa/min. Strain data were recorded after each pressure increment stabilized for a minimum of 3 min to ensure equilibrium.

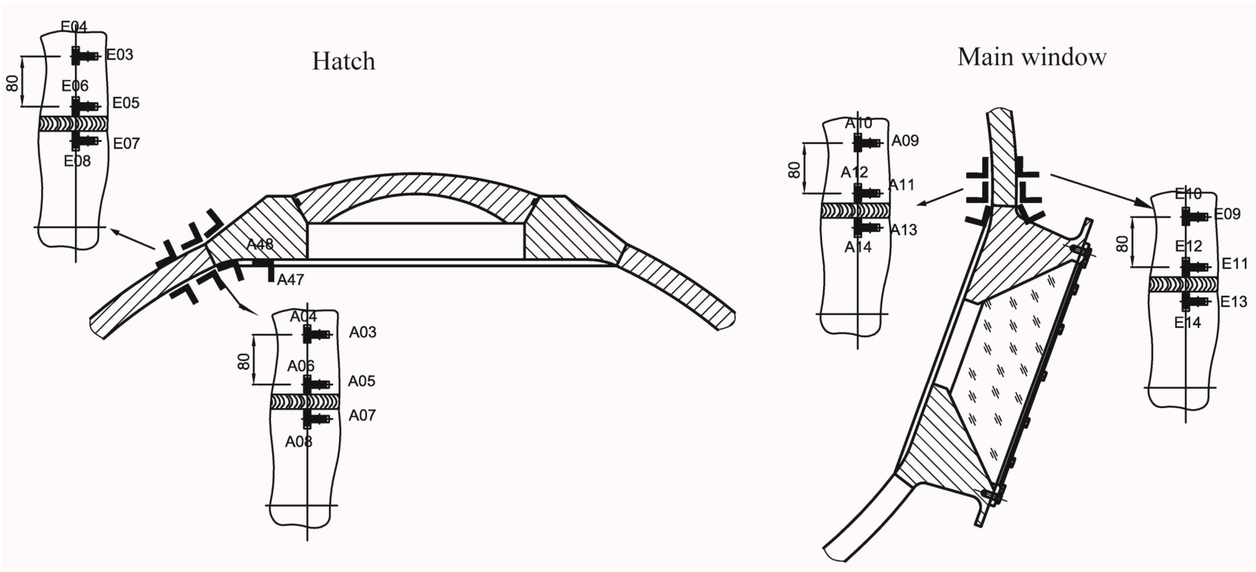

Figure 9. Arrangement of strain gauges at shell opening area.

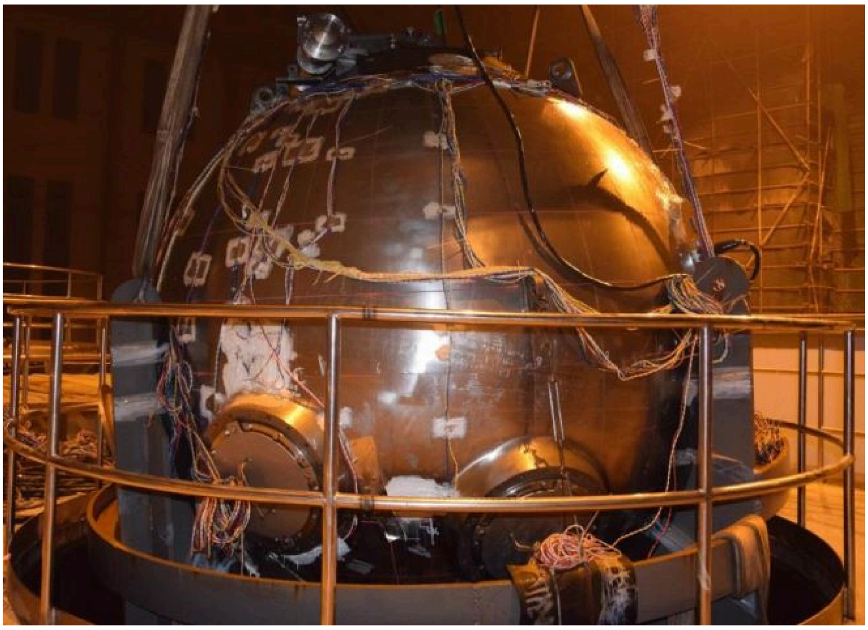

Figure 10. Test preparation.

3.2. Finite Element Analysis

The finite element analysis was applied in ABAQUS. The element type is C3D20R. The material is titanium alloy, and its density, Young's modulus and Poisson's ratio are 4510 kg/m^3, 110 GPa and 0.34, respectively. Two points, UX = UY = 0, on the Z-axis of the outer surface of the shell and one point on the X-axis, UX = UZ = 0, were applied to the boundary conditions according to the requirement of CCS illustrated in Figure 11 [31]. Mesh sensitivity was evaluated to ensure solution convergence, shown in Table 4. It can be observed that max Tresca stress of the whole model changes by less than 5%. The final spherical shell finite element model contains 38,590 elements and 190,866 nodes, ensuring a balance between computational efficiency and accuracy.

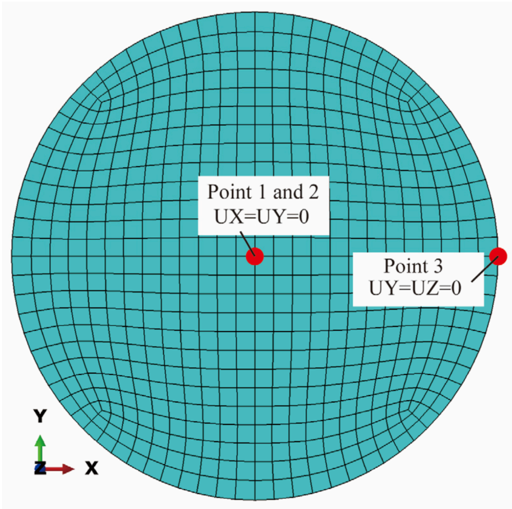

Figure 11. FEA boundary conditions.

Table 4. Mesh sensitivity analysis.

Element Size	20 mm	10 mm	5 mm
Max Tresca stress	1020 MPa	1060 MPa	1105 MPa

4. Results

Figure 12a shows the global stress distribution. And Figure 12b–d show the circumferential stress distribution at the opening area. A stress linearization procedure through the thickness was applied to obtain membrane stress at the area of interest. The FE-based SCF was defined as the ratio of the membrane stress at the reinforced opening to the membrane stress away from the shell opening.

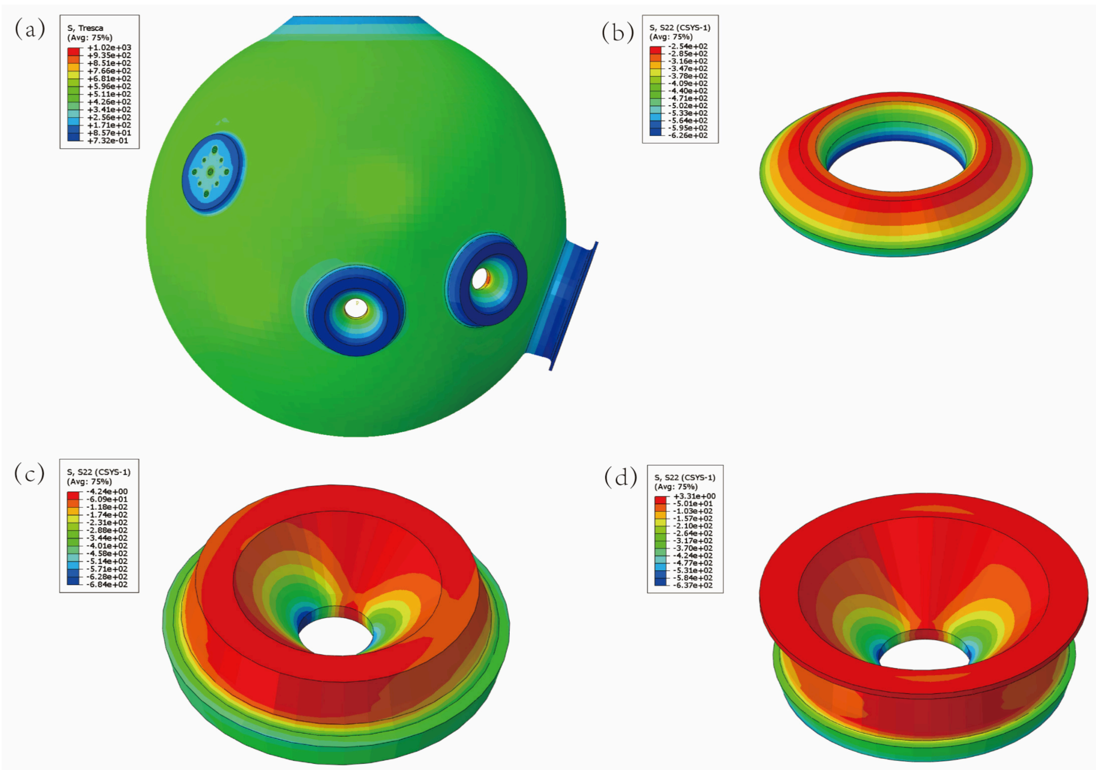

Figure 12. FEA results of opening areas: (**a**) global stress, (**b**) access hatch, (**c**) side window, (**d**) main window.

Figure 13 shows representative strain responses under the maximum test pressure of 57.5 MPa. The measured strain varies nearly linearly with external pressure and returns close to the initial value after unloading, indicating that the hull response of the structure remains elastic during the test. Membrane stresses were calculated by averaging the measured strains on the inner and outer surfaces. The tested SCF at the opening area was calculated based on measured data, as shown in Table 5. A comprehensive comparison of the SCF values obtained from the theoretical method, FEA, and the pressure tests is summarized in Table 5.

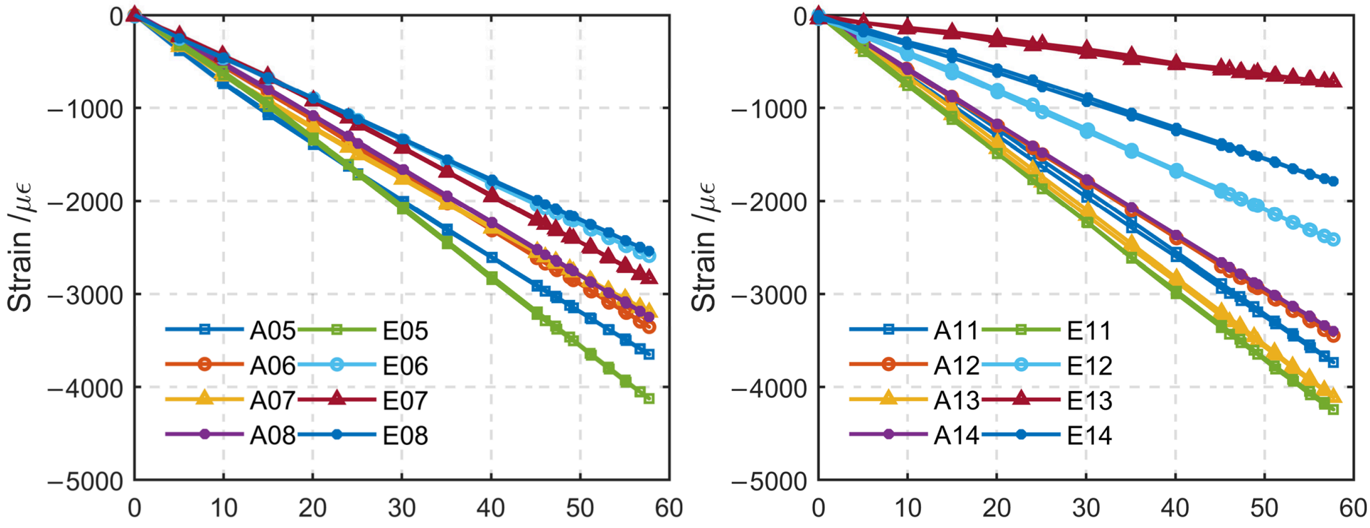

(**a**) Hatch (**b**) Main window

Figure 13. Strain response to external pressure at typical area: (**a**) Strain response at measure point of hatch. (**b**) Strain response at measure point of main window.

Table 5. Theoretical calculations and experimental results of SCF.

Material	Location	Theoretical Value	FE Analysis	Test Results	Deviation of Theoretical Value to Test Results
TA31	Hatch	1.169	1.161	1.191	1.85%
	Main window	1.274	1.207	1.221	4.34%
	Side window No. 1	1.226	1.183	1.246	1.61%
	Side window No. 2	1.226	1.183	1.195	2.59%
TC4ELI	Hatch	1.143	1.130	1.091	4.77%
	Main window	1.258	1.202	1.154	9.01%
	Side window No. 1	1.216	1.142	1.215	0.08%
	Side window No. 2	1.216	1.169	1.198	1.50%

It can be seen that the SCFs obtained by the proposed theoretical method, finite element analysis and the experiments indicate a high consistency and the deviation of most numerical results is generally within 5%, which indicates that the method proposed in this paper has high accuracy in evaluating the SCF at the opening area of spherical shells. The maximum deviation of 9.01% at the main window of the TC4ELI hull is also less than 10%, which may be attributed to the welding residual stresses in the heat-affected zone (HAZ) of the titanium alloy, which are not fully accounted for in the linear elastic theoretical model.

During manufacturing, the required tolerance for the shell thickness is (0, +1 mm), and the tolerance for the inner diameter is (−2 mm, 0). The actual manufacturing thickness of the spherical shell with TA31 alloy is 56.89 mm. Tables 6 and 7 show the influence of thickness deviation and inner diameter deviation on the SCF. From the table, it can be seen that both deviations have little influence on SCF (variations less than 0.7% and 0.02%, respectively). This suggests that the theoretical model is robust against typical manufacturing tolerance. The design parameters can effectively represent the SCF characteristics of the actual structure in the theoretical calculation. The applicability of this method has been validated with the spherical hulls with opening ratio no more than 0.32 and thickness to shell radius ratio about 0.05 in this study. Further experiments are needed to verify the applicability for spherical hulls with larger opening ratios. While this study focuses on titanium-alloy hulls, the underlying analytical principle is material-agnostic and can be adapted to other shell materials after experimental verification.

Table 6. SCF at shell opening with design shell thickness and actual shell thickness.

Location	Design Thickness t = 56 mm	Actual Thickness t = 56.89 mm	Deviation
Access Hatch	1.169	1.176	0.598%
Main window	1.274	1.282	0.628%
Side window	1.226	1.223	0.576%

Table 7. SCF at shell opening with upper and lower limits of design inside radius.

Location	Upper Limits R = 1050 mm	Lower Limits R = 1049 mm	Deviation
Access Hatch	1.169	1.1691	0.008%
Main window	1.274	1.2742	0.016%
Side window	1.226	1.2262	0.007%

5. Conclusions

This study has developed a theoretical formulation for calculating the SCF in titanium-alloy spherical hulls with opening reinforcements under external pressure. By employing a geometric transformation based on the EAC, complex geometries were successfully simplified for analytical treatment.

The proposed method was validated through comprehensive FEA and full-scale external pressure tests. The results indicate a high consistency among the theoretical predictions, finite element analysis, and experimental measurements, with most deviations remaining below 5%. The proposed method therefore provides a practical and rapid framework for evaluating the strength of opening reinforcements for underwater spherical pressure hulls.

This study is limited to spherical shells with openings and working depths similar to those in this paper. Factors like welding residual stress, manufacturing processes, and creep effects have not been fully considered. Future work will focus on extending this method to more opening types, pressure hull operation depths, manufacturing processes and different shell materials. It should be noted that the current analytical model assumes linear elastic material behavior. For ultra-deep applications where material nonlinearity or large deformation occurs, a nonlinear FEA correction factor is recommended.

Author Contributions: Methodology, L.M. and W.L.; FEA validation, X.J. and S.L.; experiment, X.J. and Y.S.; investigation, L.M. and Y.S. resources, C.Y. writing—original draft preparation, L.M. and X.J.; writing—review and editing, L.M. and W.L. All authors have read and agreed to the published version of the manuscript.

Funding: This research was funded by the National Key Research and Development Program of China (grant number: 2021YFC2800600).

Institutional Review Board Statement: Not applicable.

Informed Consent Statement: Not applicable.

Data Availability Statement: The original contributions presented in this study are included in the article. Further inquiries can be directed to the corresponding author.

Conflicts of Interest: The authors declare that they have no known competing financial interests or personal relationships that could have appeared to influence the work reported in this paper.

References

1. Qiu, Z. Design and research on a variable ballast system for deep-sea manned submersibles. *J. Mar. Sci. Appl.* **2008**, *7*, 255–260. [CrossRef]
2. Li, R.; Zhu, Y.; Fang, W.; Yin, B. Multi-Crack Interaction and Influence on the Spherical Pressure Hull for a Deep-Sea Manned Submersible. *J. Mar. Sci. Appl.* **2021**, *20*, 491–503. [CrossRef]
3. Pranesh, S.B.; Sathianarayanan, D.; Ramadass, G.A. Design standards for steel spherical pressure hull for a manned submersible. *J. Ocean Eng. Mar. Energy* **2022**, *8*, 137–151. [CrossRef]
4. Li, H.; Wang, F.; Gaidai, O.; Liu, Z.; Luo, R.; Zhang, J.; Wu, Y.; Wang, B. Reliability analysis of load capacity of spherical pressure shells considering the dispersion of material properties. *Ships Offshore Struct.* **2025**, 1–9. [CrossRef]
5. Wang, L.; Li, Y.; Sun, C.; Qiu, J.; Huang, J.; Jiang, X.; Sun, Z.; Wan, Z. Compressive creep behavior of spherical pressure hull scale model for full-ocean-depth manned submersible. *Ocean Eng.* **2022**, *266*, 112831. [CrossRef]
6. Wu, Y.; Ding, J.; Wang, F.; Sun, Z.; Zhao, M.; Wang, Y. Research on the quasi-static collapse and instantaneous implosion of the deep-sea spherical pressure hull. *Mar. Struct.* **2022**, *83*, 103191. [CrossRef]
7. Wang, L.; Ye, C.; Sun, C.; Feng, S.; Xie, X.; Gao, Y.; Zhao, K.; Li, Y.; Wan, Z. Experimental investigation on compressive dwell fatigue behavior of titanium alloy pressure hull for deep-sea manned submersibles. *Ocean Eng.* **2024**, *303*, 117646. [CrossRef]
8. Wu, Y.; Li, Y.; Luo, R.; Zhang, Z.; Wang, F.; Zhao, B.; Yang, C.; Zhang, J.; Gaidai, O. Failure analysis on fully-transparent deep-sea pressure hulls used at 2500 m depth. *Front. Mater.* **2022**, *9*, 1099610. [CrossRef]
9. Zhang, J.; Zhang, M.; Cui, W.; Tang, W.; Wang, F.; Pan, B. Elastic-plastic buckling of deep sea spherical pressure hulls. *Mar. Struct.* **2018**, *57*, 38–51. [CrossRef]
10. Liu, D.; Zhu, H.; Liu, F.; Cao, J.; Ding, Z.; Zhang, Y. Buckling failure analysis of PMMA spherical pressure hull. *Ocean Eng.* **2022**, *245*, 110465. [CrossRef]
11. Pan, B.B.; Cui, W.C.; Shen, Y.S.; Liu, T. Further study on the ultimate strength analysis of spherical pressure hulls. *Mar. Struct.* **2010**, *23*, 444–461. [CrossRef]
12. Qiu, X.; Song, H.; Huang, B.; Zhang, Z. Mechanical Properties of Hot-Stamped Spherical Shell Q235 Steel after Exposure to Elevated Temperature. *J. Mater. Civ. Eng.* **2024**, *36*, 04023537. [CrossRef]
13. Li, L.; Bao, H.; Wan, Z.; Li, Y.; Sun, K.; Luo, G. Influence of residual stress due to the equatorial weld on the ultimate strength of a Ti80 spherical pressure shell. *Int. J. Adv. Manuf. Technol.* **2021**, *116*, 1831–1841. [CrossRef]
14. Wu, C.; Cheng, Y.; Yang, N. Analysis of mechanical characteristics of conical shell with openings and fense strengthen. *Transducer Microsyst. Technol.* **2011**, *30*, 66–68. [CrossRef]
15. Hsu, C.; Liang, C.; Shiah, S.; Jen, C. A study of stress concentration effect around penetrations on curved shell and failure modes for deep-diving submersible vehicle. *Ocean Eng.* **2005**, *32*, 1098–1121. [CrossRef]
16. Zhu, Y.; Ma, Q.; Zhang, J.; Tang, W.; Dai, Y. Opening reinforcement design and buckling of spherical shell subjected to external pressure. *Int. J. Press. Vessel. Pip.* **2017**, *158*, 29–36. [CrossRef]
17. Pankratova, N.D.; Pol'chuk, V.B. Stress-strain state of an open spherical shell of a medium thickness. *Strength Mater.* **2006**, *38*, 498–505. [CrossRef]
18. Ismail, M.S.; Mahmud, J.; Muhammad al-Attas, S.M.; Purbolaksono, J.; Błachut, J. Buckling stability of steel spherical shells: A numerical investigation under combined external pressure, geometric imperfections, and thermal loading. *Int. J. Press. Vessel. Pip.* **2025**, *218*, 105620. [CrossRef]
19. Ismail, M.S.; Ifayefunmi, O.; Fadzullah, S.H.S.M. Buckling of imperfect cylinder-cone-cylinder transition under axial compression. *Thin-Walled Struct.* **2019**, *144*, 106250. [CrossRef]
20. Wagner, H.N.R.; Hühne, C.; Zhang, J.; Tang, W. On the imperfection sensitivity and design of spherical domes under external pressure. *Int. J. Press. Vessel. Pip.* **2020**, *179*, 104015. [CrossRef]
21. Ismail, M.S.; Ifayefunmi, O.; Fadzullah, S.H.S.M.; Johar, M. Buckling of imperfect cone-cylinder transition subjected to external pressure. *Int. J. Press. Vessel. Pip.* **2020**, *187*, 104173. [CrossRef]
22. Wagner, H.N.R.; Hühne, C.; Zhang, J.; Tang, W.; Khakimova, R. Geometric imperfection and lower-bound analysis of spherical shells under external pressure. *Thin-Walled Struct.* **2019**, *143*, 106195. [CrossRef]

23. Guo, Y.; Teng, Y.; Liu, G.; Jiao, T. Numerical study on creep-fatigue damage of titanium alloy pressure shell considering the effect of welding residual stresses. *Thin-Walled Struct.* **2025**, *209*, 112953. [CrossRef]
24. Yu, C.; Guo, Q.; Gong, X.; Yang, Y.; Zhang, J. Fatigue life assessment of pressure hull of deep-sea submergence vehicle. *Ocean Eng.* **2022**, *245*, 110528. [CrossRef]
25. Yongmei, Z.; Junjie, B.; Lihui, W.; Tianyi, S.; Hongzhang, P.; Hao, W. Fatigue crack propagation characteristics of segmented egg-shaped pressure shells. *Ocean Eng.* **2023**, *287*, 115940. [CrossRef]
26. Millet, B.; Ebrahimi, K.; Lu, J.; Kirkpatrick, K.; Mosher, B. A Study of the Conservatism in ASME BPVC Section VIII Division 2 Opening Design for External Pressure. In Proceedings of the ASME 2019 Pressure Vessels & Piping Conference, San Antonio, TX, USA, 14–19 July 2019.
27. Calligeros, D. Review of Reinforcement of Pressure Vessel Openings Under External Pressure. Master's Thesis, The University of Queensland, Brisbane, Australia, 2008.
28. Xu, B.; Zhu, B.; Ouyang, L.; Pei, J. *Theory and Experiments on Modern Submarine Structure Strength*; National Defense Industry Press: Beijing, China, 2007.
29. Pranesh, B.; Sathianarayanan, D.; Ramesh, S.; Ramadass, G.A. Structural Reinforcement of Viewports in Spherical Pressure Hull for Manned Subersibles. *Mar. Technol. Soc. J.* **2014**, *48*, 17–24. [CrossRef]
30. Ma, Q.; Zhu, Y.; Liang, W.; Zhang, J. Buckling and strength of an externally pressurized spherical shell with reinforced opening. *Int. J. Press. Vessel. Pip.* **2018**, *165*, 11–19. [CrossRef]
31. China Classification Society. Rules for the Classification of Diving Systems and Submersibles. 2018. Available online: https://www.ccs.org.cn/ccswzen/specialDetail?id=201910000000003438 (accessed on 25 October 2025).
32. Xu, B.; Pei, J.; Zhu, B. *Theory and Experiments on Shell Opening*; National Defense Industry Press: Beijing, China, 1987.